A&A 466, 755–762 (2007)
DOI: 10.1051/0004-6361:20077056

Astronomy & Astrophysics

Dielectronic recombination data for dynamic finite-density plasmas

XII. The helium isoelectronic sequence

M. A. Bautista[1] and N. R. Badnell[2]

[1] Centro de Física, IVIC, PoBox 21827, Caracas 1020A, Venezuela
e-mail: bautista@kant.ivic.ve
[2] Department of Physics, University of Strathclyde, Glasgow G4 0NG, UK

Received 4 January 2007 / Accepted 29 January 2007

ABSTRACT

We report on total and final-state resolved partial dielectronic recombination data for helium-like ions forming lithium-like ions. The calculations consider ions of Li, Be, B, C, N, O, F, Ne, Na, Mg, Al, Si, P, S, Cl, Ar, K, Ca, Sc, Ti, V, Cr, Mn, Fe, Co, Ni, Zn, Kr, Mo, and Xe. The results are discussed and compared with available experimental data and with previous calculations. Our archived datasets include both total and level-specific DR rate coefficients. The total ion rate coefficients are provided both in tabulated form and as analytical fits for easy implementation into spectral modelling codes. We employ the level specific rate coefficients in constructing detailed spectral models of Li-like ions including the combined effects of collisional excitation and recombination. The results from these models are compared with the those pure collisional excitation models under typical conditions of low density plasmas. This work is part of an assembly of a dielectronic recombination database for modelling of finite-density plasmas.

Key words. atomic data – atomic processes – line: formation

1. Introduction

The electron-ion recombination process in plasmas spans a wide range of physical conditions. This process governs the ionization stage of the plasma when it is not in local thermodynamic equilibrium. It also gives rise to spectral emission which can be used for diagnostic purposes. It is thus of fundamental practical interest in the study of astrophysical plasmas, interstellar chemistry, shock waves, laboratory and laser produced plasmas, electron cooling of heavy ion beams in storage rings, discharges, magnetic and laser confined fusion devices, and in electron-beam ion-trap experiments.

Historically, the recombination process is divided into radiative recombination (RR) and dielectronic recombination (DR). The former results from direct capture of a free electron into a bound state of the recombining ion. The rate coefficients for such a mechanism are calculated from direct, non-resonant, photoionization cross sections. The DR mechanism is one whereby the free electron is captured into an autoionizing state of the recombined ion, followed by radiative decay to a bound level. Thus, DR rate coefficients can be computed by explicit accounting of all autoionizing levels of the recombined ion and their respective autoionization and radiative rates (e.g. Burgess 1964, 1965). Under low densities and weak radiation fields, where practically all excited ions cascade to their ground states in times that are short enough that collisional transitions and stimulated radiative transitions from excited states can be neglected, DR can be viewed as the contribution of autoionizing resonances of photoionization cross sections. This approach has led to extensive calculations of total and level-specific recombination rate coefficients for all ions of C, N and O (Nahar & Pradhan 1997; Nahar 1999).

However, there are numerous practical applications in which radiative and dielectronic recombination must be treated separately for explicit treatment of the collisional-radiative population of levels and the related radiation spectra. Relatively high electron densities are present in a variety of laboratory plasmas, for example, in fusion plasmas (Summers et al. 2002) and in Z-pinch photoionized plasmas (e.g. Heeter et al. 2000), and in astrophysical plasmas, like in the accretion disks of low-mass X-ray binaries (Bautista et al. 1998) and possibly in the so-called warm absorber in active galactic nuclei (Kallman & Bautista 2001). In these cases, radiative cascades from autoionizing levels may be interrupted by electron collisions that further redistribute the population and reduce the effective dielectronic recombination rate. The onset of these density effects depends on ion charge, but can be important even at electron densities as low as 10^8 cm^{-3}, typical of solar corona. At higher densities, around 10^{14} cm^{-3}, density effects can interrupt the two-step dielectronic processes altogether.

Partial dielectronic recombination rate coefficients are also needed in the study of particular physical problems, for example: at low temperatures, where only a few autoionizing states contribute significantly (Nussbaumer & Storey 1983); satellite line spectra, where decay of autoionizing levels yield observable spectral lines (e.g. Bely-Dubau et al. 1979); laser produced plasmas, where the electron density and/or charge state is high enough that the non-LTE populations are concentrated in a limited number of low-lying states (e.g. Abdallah & Clark 1994).

The spectral emission of highly charged He-like ions has been used heavily in the diagnostic analysis of astrophysical plasmas for some time. Its importance is due to the fact that the ionization equilibrium fractional abundance of the He-like stage spans a wide temperature range. This leads to large spectral intensities in temperature-stratified plasmas such as the solar chromosphere and corona. Collectively, the He-like ionization stage of elements span virtually all temperature regimes of a plasma. Thus, a particular zone of a plasma may be studied by the emission lines of the He-like ion which exists there.

The importance of He-like ions has led to extensive studies of their collisional properties. Here we focus on DR as part of the program to assemble a level-resolved DR database necessary for modelling dynamic and/or finite density plasmas (Badnell et al. 2003). The present work archives final state-resolved DR coefficients, which are necessary for modelling plasmas at densities for which the coronal approximation is not valid, for both the ground and metastable initial states, which is necessary for modelling dynamic plasmas whose metastable populations are not in quasi-static equilibrium with the ground state. A complementary RR database has also been assembled (Badnell 2006a).

A number of researchers have calculated total DR rate coefficients for such an important sequence as the He-like, however significant uncertainties remain. Firstly, much of the data currently available was computed in *LS* -coupling and that is an important source of uncertainty. Savin & Laming (2002), Badnell (1988), and Gorczyca & Badnell (1996) point out that, in the absence of spin-orbit interaction, this approximation misses a fraction of the autoionizing levels contributing to the DR process. Storage ring measurements and relativistic many-body perturbation calculations have verified the importance fine structure transitions (Mannervik et al. 1998). As for calculations that take relativistic effects into account, Chen (1986, 1988) carried out multiconfiguration Dirac-Fock calculations for DR recombination of various ions of the helium isoelectronic sequence. The results of Chen agree within 10% with the MCBP rate coefficients of Badnell & Pindzola (1989) for O^{6+}. Mazzota et al. (1998, M98 hereafter) provided parametric fit coefficients of Chen and of Pindzola & Badnell (1992) for Be^{2+} and B^{3+}. M98 also interpolated along the isoelectronic sequence for missing ions. The review of Savin & Laming (2002) concludes, based on comparisons between various calculations and experiments in the literature, that the most reliable dataset is that of M98, at least for temperatures above 10^5 K. For lower temperatures Chen (1986, 1988) did not give any results, thus the parametric fits of M98. do not have the correct behaviour at temperatures typical of photoionized plasmas. Recently, Gu (2003) computed new DR rate coefficients for Mg, Si, S, Ar, Ca, Fe, and Ni using a fully relativistic distorted wave approach. His rates for the He-like ions are in very close agreement with those of Chen (1986, 1988).

Experimental measurements have been reported for DR of various ions of the He-like sequence into the Li-like stage, e.g. of Li^+ (Závodszky et al. 1998; Saghiri et al. 1999), of C^{4+} (Andersen et al. 1989, 1990; Kilgus et al. 1990, 1993; Schuch et al. 1997), O^{6+} (Andersen et al. 1989, 1990), Ne^{8+} (Zong et al. 1998), Si^{12+} (Kenntner et al. 1995; Bartsch et al. 1997), Ar^{16+} (Ali et al. 1990, 1991; Dewitt et al. 1991), and Ti^{20+} (O'Rourke et al. 2004), Fe^{24+} (Beiersdorfer et al. 1992), Ni^{26+} and Mo^{40+} and Ba^{54+} (Knapp et al. 1993). Owing to instrumental corrections it is often difficult to compare directly with experimental measurements of DR cross sections. Notwithstanding, in this paper we present some comparisons with our present theoretical results.

As for level specific recombination rate coefficients, these have been reported as part of specific applications for isolated ions, but to the best of our knowledge the present one is the first comprehensive publication of intermediate coupling, level-resolved, practically tabulated and accessible DR rate coefficients for the He isoelectronic sequence.

Finally, another important possible application of the underlying physics and modelling codes, although beyond the scope of the present work, is in regards to He-like DR satellite lines, which are a widely used temperature diagnostic in astrophysical (e.g. Bautista & Kallman 2000, and references therein) and fusion (Marchuk et al. 2004) plasmas. Here, information is required about the population of the autoionizing levels.

The remainder of this paper is organized as follows: in the next section we describe the theoretical methods used and describe our calculations. In Sect. 3 we present the results for both partial total DR data and present some relevant comparisons with experimental data and compare them with the results of previous calculations. New spectral models for Li-like models that use the level specific recombination rates are described in Sect. 4, and some representative results are presented and compared with those from pure collisional excitation models. Finally, Sect. 5 summarizes the work and presents our conclusions.

2. Theory and calculations

The theoretical methods employed for the present project are explained in detail by Badnell et al. (2003), thus we only outline the main points here. We employ the code AUTOSTRUCTURE (Badnell 1986, 1997; Badnell & Pindzola 1989), which is an extension of the atomic structure program SUPERSTRUCTURE by (Eissner et al. 1974). The code allows for the calculation of LS-coupling or intermediate coupling level energies, radiative and Auger rates in a Breit-Pauli relativistic framework. Single electron orbitals, $P_{\rm nl}(r)$, are constructed by diagonalizing the non-relativistic Hamiltonian, $H_{\rm nr}$, within a statistical Thomas-Fermi-Dirac model potential $V(\lambda_{\rm nl})$ (Eissner & Nussbaumer 1969). The $\lambda_{\rm nl}$ scaling parameters are optimized variationally by minimizing a weighted sum of the *LS* term energies. The latter are represented by configuration-interaction (CI) wavefunctions of the type

$$\Psi = \sum_i c_i \phi_i. \quad (1)$$

The quality of such a representation can be assessed by the accuracy of the computed energies of autoionizing levels of the target-plus-electron system. Table 1 contains a comparison between experimental energies, obtained from the energy levels database of the National Institute for Standards and Technology (NIST 2002), and those from the present calculations. One finds that the theoretical energies are within ~2% and <0.2% of the experimental energies for Li^0 and Fe^{23+}, respectively. The fact that the agreement for Fe^{23+} is better than for Li^0 is expected as term interaction becomes much more difficult to represent for neutral systems than for highly ionized ions. Nevertheless, such levels of agreement between present calculations and experiment are encouraging.

Continuum wavefunctions are constructed within the distorted-wave approximation, and the autoionization rates are computed in the isolated resonance approximation. Interference between RR and DR are neglected, which is expected to be a good approximation for the cases of interest here (Pindzola et al. 1992). Relativistic fine-structure levels and rates are obtained by diagonalizing the Breit-Pauli Hamiltonian in intermediate coupling. Both one- and two-body operators–fine structure and non-fine structure–have been fully implemented to order α^2 where α is the fine-structure constant.

The large array of autoionization and radiative rates computed with AUTOSTRUCTURE was processed with the code ADASDR (Badnell et al. 2003) to produce partial and total dielectronic recombination rate coefficients. Recombination rate coefficients were produced in both *LS* -coupling and intermediate coupling (IC) for the species from Li^0 through Ni^{25+}, and in IC only for Zn, Kr, Mo, and Xe. It is important to note that for the

Table 1. Comparisons between calculated and experimentally determined energies (in Ry) for autoionizing levels of Li^0 and Fe^{23+}.

Li^0 Config.	Term	$2J$	$E_{exp.}$	$E_{theo.}$
$1s^2\ 2s$	^2S	1	0.00000	0.00
1s 2s 2p	$^4P^\circ$	1	4.22391	4.31446
		3	4.22391	4.31448
		5	4.22391	4.31452
1s 2p(1P°)2s	^2P	1	4.32989	4.40966
		3	4.32989	4.40969
1s $2p^2$	^4P	1	4.46922	4.49300
		3	4.46922	4.49302
		5	4.46922	4.49305
1s 2p2	^2P	1	4.52745	4.57840
		3	4.52745	4.57844
Fe^{23+} Config.	Term	$2J$	$E_{exp.}$	$E_{theo.}$
1s2 2s	^2S	1	0.000	0.000
$1s(^2S)2s2p(^3P^\circ)$	$^4P^\circ$	3	486.5	487.221
$1s(^2S)2s2p(^3P^\circ)$	$^2P^\circ$	1	488.95	489.794
		3	489.82	490.599
$1s2p^2$	^4P	1	490.31	490.886
		3	490.96	491.498
		5	491.51	492.055
$1s(^2S)2s2p(^1P^\circ)$	$^2P^\circ$	1	490.66	491.604
		3	491.20	491.776
$1s2p^2$	^2D	3	492.70	493.416
		5	493.23	493.942
$1s2p^2$	^2P	1	492.78	493.568
		3	494.30	494.915
$1s2p^2$	^2S	1	495.59	496.335

former set of ions we employ non-relativistic solutions of the radial equations, while for the heavier ions we use semi-relativistic wavefunctions (i.e. mass-velocity and Darwin operators are included in the solution of the radial equations).

Dielectronic recombination from the ground level of He-like ions proceeds through electron capture to $1s2lnl'$ autoionizing states, $n = 1 \rightarrow 2$ core excitation, followed by radiative stabilization (i.e. recombination) and autoionization (that yields resonance collisional excitation). This processes can be written as

$$1s^2 + e^- \rightarrow \left\{ \begin{array}{l} 1s2snl \\ 1s2pnl \end{array} \right\} \begin{array}{l} \nearrow \left\{ \begin{array}{l} 1s^2 2s + h\nu \\ 1s^2 2p + h\nu \\ 1s^2 nl + h\nu \end{array} \right\} \text{(DR)} \\ \searrow \left\{ \begin{array}{l} 1s^2 + e^- \\ 1s2s + e^- \\ 1s2p + e^- \\ 1snl + e^- \end{array} \right\} \text{(CE)} \end{array} \quad . \tag{2}$$

In the present calculation we explicitly included configurations up to $n = 15$ and angular momenta $0 \le l \le n-1$. Then, higher states up to $n = 1000$ were taken into account through an interpolation procedure described by Badnell et al. (2003). In addition to the decay channels of autoionizing states described above, we have studied radiative transitions among autoionizing states which were found to be important to high n resonances in the photorecombination cross section of Fe^{17+}

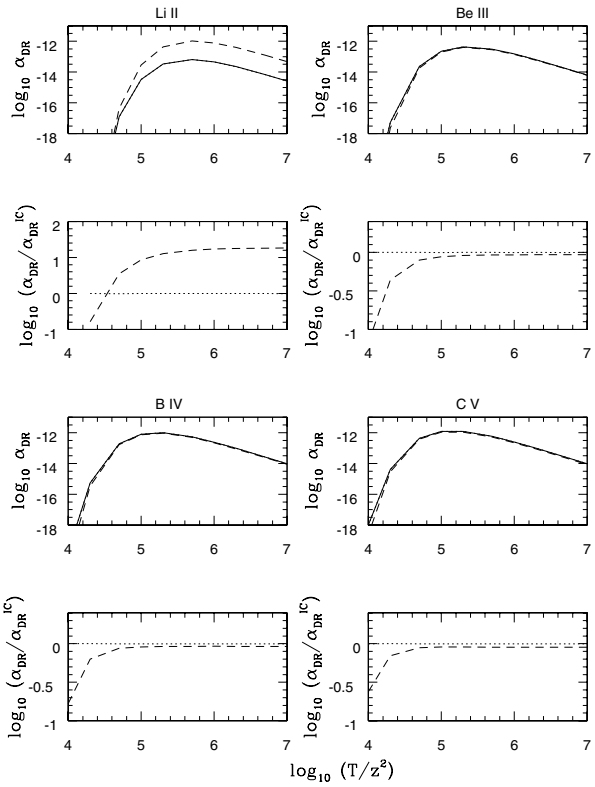

Fig. 1. Logarithm of the DR recombination rate coefficients (in $cm^3\ s^{-1}$) vs. the logarithm of the T/z^2, where z is the effective charge of the He-like ion. For each ion we show two panels. The upper one shows the logarithm of the DR and the lower panel plots ratios of DR rate coefficients to the present IC results. The different data plotted are: present IC results (solid lines), present *LS* results (dotted lines), data from M98 (dashed lines).

(Gorczyca et al. 2002). This process, which can be described as

$$\left\{ \begin{array}{l} 1s2snl \\ 1s2pnl \end{array} \right\} \rightarrow \left\{ \begin{array}{l} 1s2sn'l' \\ 1s2pn'l' \end{array} \right\} \begin{array}{l} \nearrow \left\{ \begin{array}{l} 1s^2 2s + h\nu \\ 1s^2 2p + h\nu \\ 1s^2 n'l' + h\nu \end{array} \right\} \\ \searrow \left\{ \begin{array}{l} 1s^2 + e^- \\ 1s2s + e^- \\ 1s2p + e^- \\ 1sn'l' + e^- \end{array} \right\} \end{array} \tag{3}$$

was found to make only a small contribution, $\lesssim 2\%$, to the total recombination rate coefficients of He-like ions.

Finally, we have looked at the contribution from $n = 1 \rightarrow 3$ core excitations for C, Fe and Xe but find that the $n = 3 \rightarrow 2$ alternative autoionization pathway efficiently suppresses it. It contributes no more than 2%, 3% and 5%, respectively, of the total DR rate coefficient at its peak.

3. Results

Total and final-state level-resolved dielectronic recombination rate coefficients were calculated for recombination from the helium isoelectronic ions from Li to Ni, and for Zn, Kr, Mo, Kr. We consider recombination from the $1s^2\ ^1S$ ground level of the He-like recombining ion and the calculations are carried out in both *LS* and intermediate coupling schemes.

Figure 1 shows total recombination coefficients for a sample of ions for a wide range of temperatures and compares the IC results with the *LS* ones and with the results of previous data from

Table 2. Comparison between IC and *LS* state-specific DR rate coefficients for Fe^{24+}.

	IC	*LS*	2*J*	IC	*LS*
2^2S	1.41(−14)	1.68(−14)	1	1.41(−14)	1.41(−14)
2^2P°	5.56(−14)	5.55(−14)	1	1.53(−14)	1.85(−14)
			3	4.03(−14)	3.70(−14)
3^2S	2.12(−15)	4.64(−16)	1	2.12(−15)	2.12(−15)
3^2P°	1.29(−14)	1.34(−14)	1	4.23(−15)	4.47(−15)
			3	8.71(−15)	8.94(−15)
3^2D	7.17(−15)	7.42(−15)	3	1.70(−15)	2.97(−15)
			5	5.48(−15)	4.45(−15)
4^2S	7.38(−16)	9.81(−17)	1	7.38(−16)	7.38(−16)
4^2P°	4.88(−15)	3.59(−15)	1	1.67(−15)	1.20(−15)
			3	3.21(−15)	2.39(−15)
4^2D	3.23(−15)	3.41(−15)	3	6.61(−16)	1.36(−15)
			5	2.57(−15)	2.05(−15)
4^2F°	4.83(−16)	5.16(−16)	5	1.95(−16)	2.21(−16)
			7	2.88(−16)	2.95(−16)
5^2S	3.30(−16)	3.19(−17)	1	3.30(−16)	3.19(−17)
5^2P°	2.46(−15)	1.65(−15)	1	7.56(−16)	5.50(−16)
			3	1.70(−15)	1.10(−15)
5^2D	1.61(−15)	1.67(−15)	3	3.33(−16)	6.67(−16)
			5	1.28(−15)	1.00(−15)
5^2F°	2.80(−16)	3.12(−16)	5	1.15(−16)	1.34(−16)
			7	2.69(−17)	1.78(−16)
5^2G	2.13(−16)	7.23(−17)	7	1.78(−16)	3.21(−17)
			9	3.50(−17)	4.02(−17)

Columns 2 and 3 compare the rate coefficients per $LS\pi$ multiplet. Columns 5 and 6 compare the computed level specific rate coefficients with those obtained by algebraic splitting of non-relativistic *LS* rate coefficients. Column 4 indicates the 2*J* value for each level.

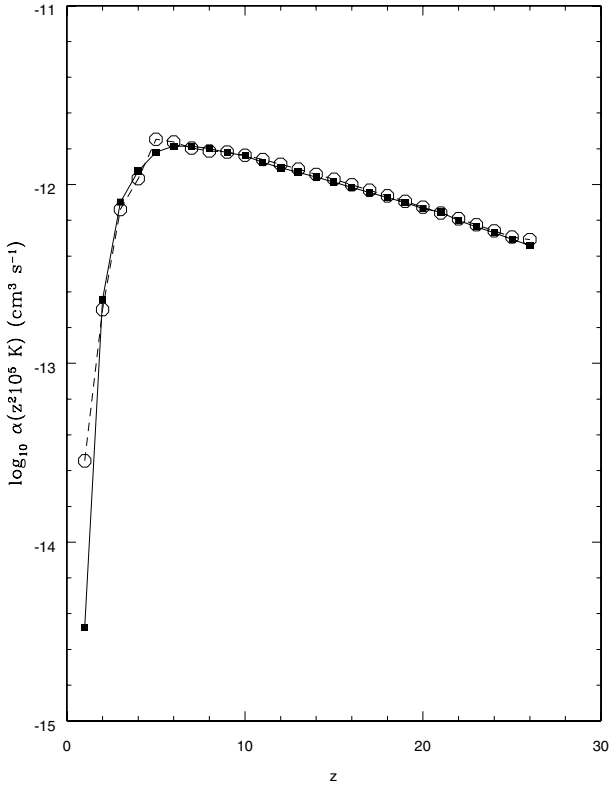

Fig. 2. Total DR rate coefficients (in $cm^3\ s^{-1}$) at temperatures of $10^5\ z^2$ K vs. the effective ion charge z. The solid line and filled dots indicate the present results and the dashed line and open dots represent data from M98.

M98. In this figure there are two plots for each ion: an upper plot for the recombination rate coefficients and a lower plot with the ratio of *LS* rate coefficients and other author's rates to the current IC results. One finds very good agreement, within ∼5%, between IC and *LS* total rate coefficients in the vicinity of the DR peak for ions up to Ni^{26+}. While relativistic effects and IC yields much more DR channels, which may change the DR detailed cross section, the accumulated effect of individual rates to the total DR rate differ little from the *LS* coupling rate.

Nonetheless, spin-orbit coupling effects are important to level-specific DR of medium and highly ionized species. As expected, such effects are negligible for neutral and near neutral ions, but they grow rapidly with nuclear charge. We find that IC effects on state-specific rates become important, ≥10%, for Mg^{10+} and heavier ions. To illustrate the importance of IC effects we show in Table 2 a comparison between *LS* and IC state specific DR rates for Fe^{24+}. One finds significant coupling between $L = 0$ and $L = 2$ even states, $L = 1$ and $L = 3$ odd states, and $L = 2$ and $L = 4$ even states. These coupling effects result in up to one order of magnitude changes in the DR rates of the lower angular momentum states. Another interesting finding is that the splitting of rates from multiplets onto fine structure levels departs from statistical weights branching ratios. These results clearly point to the need for the use of IC DR rate coefficients in spectral modelling applications, while the use *LS*-coupling DR data could led to significant errors.

With the exception of lithium, our results agree well, ∼10%, with those in M98 in the region near the DR peak and for higher temperatures. This agreement is generally worse for lower charge ions and better for the highly charged ions. For lower temperatures, $T < 10^5\ z^2$ K, there are large differences due to the fact that Chen (1986, 1988) did not provide results in this range.

Another comparison between the present results and those in M98 is presented in Fig. 2. Here we plot the logarithm of the DR rate at a temperature of $10^5\ z^2$ K (near the DR maxima) for all ions, against the ion's effective charge $z = Z - 2$. This plot shows good agreement, within 20%, between the present results and most of the M98 data, although in the M98 data the progression with z looks rather rough below oxygen ($z = 6$). A notable discrepancy occurs for Li^+, for which the present results are about a factor nine lower than the M98 data, which was derived by M98 through extrapolation along the isoelectronic sequence. This difference supports the comparisons of Fig. 1 in the sense that the M98 rates for Li^+ are overestimated by as much as one order of magnitude.

3.1. Comparisons with experiment

The first (single-pass) DR measurements using an electron-cooler were carried-out by Andersen et al. (1989, 1990) on metastable He-like C and O. Excellent agreement with these measurements was obtained by Badnell et al. (1990) using AUTOSTRUCTURE. Measurements and calculations of DR from the ground state of C^{4+} were made by Kilgus et al. (1993). Subsequent radiation damped *R*-matrix calculations by Price (1997) and by Zhang et al. (1999) are in good accord with them. Much higher energy resolution measurements on C^{4+} were made by Schuch et al. (1997). In Figs. 3 and 4 we

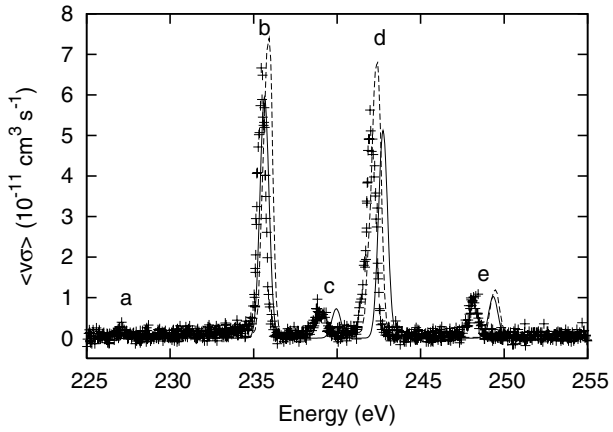

Fig. 3. Velocity-weighted DR cross sections for C^{4+}. Pluses, from the experiment by Schuch et al. (1997); dashed line, radiation damped R-matrix results of Price (1997); solid line, present Breit-Pauli perturbation theory results. Both sets of theoretical results were convoluted with the experimental velocity distribution: $kT_{\|} = 0.15$ meV and $kT \perp = 10$ meV. Peak "a" consists of the autoionizing resonance $1s2s^2\,{}^2S$, peak "b" of $1s(2s2p^3P)\,{}^2P$, "c" of $1s(2s2p^1P)\,{}^2P$, "d" of $1s2p^2\,{}^2D$ and peak "e" of $1s2p^2\,{}^2S$.

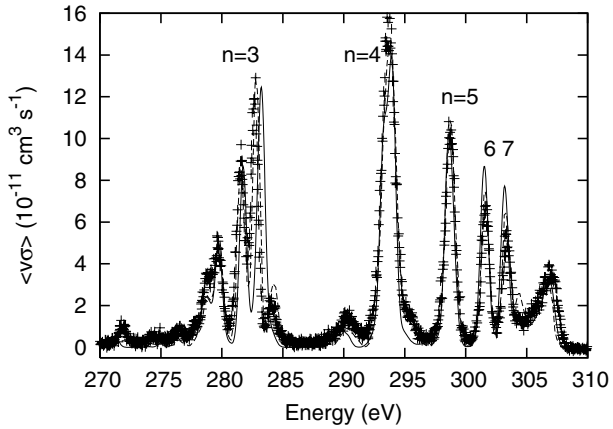

Fig. 4. As Fig. 3, but for the KLn, $n \geq 3$, resonance groups.

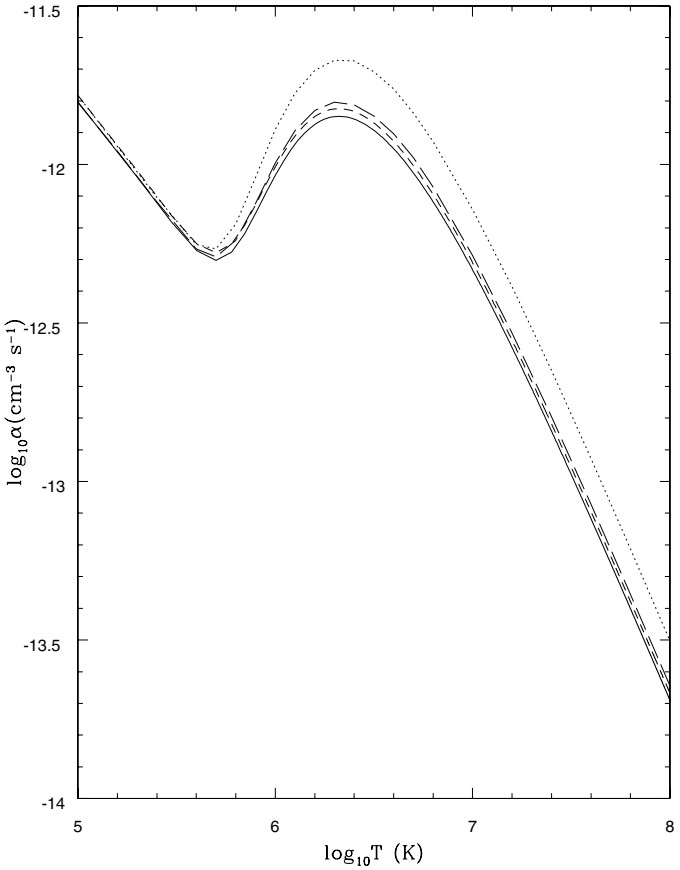

Fig. 5. Logarithm of the total (RR+DR) recombination rate coefficients of C^{4+} vs. $\log_{10} T$. The various curves represent the addition of present DR results (solid curve) and experimentally derived DR rate coefficients of Savin (1999, short dashed curve) with RR values of Verner & Ferland (1996). Other curved are the total recombination rate coefficients of Nahar et al. (2000, long-dashed curve) and Nahar & Pradhan (1997, dotted curve).

compare our AUTOSTRUCTURE results with those of Schuch et al. (1997) and with the radiation damped R-matrix results of Price (1997). There is good agreement between all three sets of results, with the R-matrix results perhaps in marginally better agreement with the observed. Measurements and calculations (using AUTOSTRUCTURE) for metastable N, F and Si were made by Andersen et al. (1992) and the two were in good agreement, although the uncertainties were large for Si. There was a low energy resolution measurement of DR from the ground and metastable states of Li^+ by Závodszky et al. (1998) and a higher energy resolution measurement, but still with a relatively weak signal, by Saghiri et al. (1999), both were in broad accord with theory (Price 1997).

Savin (1999) obtained total DR rate coefficients for C^{4+} from experimental resonance strengths and compared these rate coefficients with the R-matrix computed DR+RR rate coefficients of Nahar & Pradhan (1997). Figure 5 compares these rate coefficients with the present results and those of Nahar et al. (2000). In order to compare DR rate coefficients with the R-matrix DR+RR results of Nahar and collaborators, the earlier DR data was added to RR rate coefficients as taken from the fits of Verner & Ferland (1996). We find very good agreement, within 5%, between the experimentaly derived data and those of Nahar et al. (2000) and the present results. The earlier R-matrix calculation of Nahar & Pradhan (1997) that did not take radiation damping of resonances into account is overestimated by ∼50% in the temperature range dominated by DR. Radiation damped R-matrix recombination rate coefficients have only been published for He-like carbon (Nahar et al. 2000), oxygen (Nahar 1999) and iron (Nahar et al. 2001).

Extensive comparisons between the Breit-Pauli results of perturbation theory and of radiation damped R-matrix calculations have also been carried-out for the DR of He-like Fe by Gorczyca & Badnell (1997), Badnell et al. (1998) and Zhang et al. (1999) for the KLn DR resonances for $n = 2$–6. The conclusion of these works was that there was very close agreement between the results of perturbation theory and R-matrix calculations, to within a few percent. Indeed, for KLO and KLP the differences between R-matrix results from the two groups was greater than the difference between perturbation theory and R-matrix results from within the two groups. Good agreement was also obtained with the EBIT measurements of Beiersdorfer et al. (1992) for the KLL resonance group.

Table 3. Fit coefficients for calculating $\alpha^{\rm DR}$. C_i are in units of $K^{3/2}$ cm^3 s^{-1} and E_i are in units of K.

Z	C_1	C_2	C_3	C_4	E_1	E_2	E_3	E_4
3	2.941E-05	6.068E-05	–7.753E-07		6.345E+05	7.024E+05	8.271E+05	
4	1.942E-04	1.485E-03	1.320E-05		1.185E+06	1.377E+06	1.904E+06	
5	9.375E-04	7.606E-03	–2.683E-04		1.913E+06	2.319E+06	2.732E+06	
6	2.646E-03	1.762E-02	–7.843E-04		2.804E+06	3.485E+06	4.324E+06	
7	5.761E-03	3.434E-02	–1.660E-03		3.860E+06	4.883E+06	6.259E+06	
8	6.135E-02	1.968E-04			6.113E+06	3.656E+07		
9	1.006E-02	6.743E-02	1.034E-02		6.330E+06	7.859E+06	9.755E+06	
10	1.552E-02	9.008E-02	1.182E-02		7.845E+06	9.803E+06	1.209E+07	
11	2.228E-02	1.133E-01	1.296E-02		9.521E+06	1.195E+07	1.502E+07	
12	3.067E-02	1.375E-01	1.347E-02		1.136E+07	1.431E+07	1.762E+07	
13	4.093E-02	1.618E-01	1.332E-02		1.336E+07	1.689E+07	2.091E+07	
14	5.318E-02	1.874E-01	1.227E-02	7.173E-04	1.552E+07	1.969E+07	2.532E+07	2.696E+08
15	6.756E-02	2.122E-01	1.292E-02		1.784E+07	2.270E+07	2.867E+07	
16	8.410E-02	2.381E-01	1.065E-02	1.049E-03	2.032E+07	2.592E+07	3.206E+07	2.016E+08
17	1.172E-01	6.677E-01	–4.111E-01		2.302E+07	3.470E+07	3.817E+07	
18	1.220E-01	2.795E-01	1.569E-02		2.576E+07	3.288E+07	4.360E+07	
19	1.598E-01	3.107E-01	–1.177E-02		2.879E+07	3.822E+07	5.308E+07	
20	1.659E-01	3.186E-01	1.801E-02		3.186E+07	4.085E+07	5.068E+07	
21	2.046E-01	6.275E-01	–2.876E-01		3.521E+07	5.102E+07	5.741E+07	
22	2.099E-01	3.706E-01	1.402E-03		3.861E+07	5.000E+07	3.341E+08	
23	2.464E-01	3.773E-01	–8.236E-03		4.229E+07	5.601E+07	8.486E+07	
24	2.486E-01	3.758E-01	2.241E-02	6.461E-04	4.601E+07	5.914E+07	7.241E+07	3.231E+08
25	2.977E-01	1.039E+00	–6.600E-01		5.018E+07	7.823E+07	8.614E+07	
26	2.676E-01	4.097E-01	2.990E-02		5.394E+07	6.854E+07	9.651E+07	
27	3.096E-01	5.586E-01	–1.398E-01		5.844E+07	8.074E+07	9.415E+07	
28	2.934E-01	4.324E-01	2.800E-02		6.268E+07	7.990E+07	1.212E+08	
29	3.452E-01	6.344E-01	–2.055E-01		6.767E+07	9.628E+07	1.123E+08	
30	3.493E-01	4.849E-01	1.422E-02		7.239E+07	9.475E+07	9.542E+07	
36	3.917E-01	6.921E-01	–1.344E-01		1.045E+08	1.403E+08	1.532E+08	
42	4.624E-01	5.046E-01	5.396E-02	2.056E-03	1.434E+08	1.833E+08	2.282E+08	9.195E+08
54	5.389E-01	5.238E-01	4.275E-02	2.568E-03	2.415E+08	3.136E+08	3.732E+08	1.541E+09

3.2. Fits to total DR rate coefficients

For convenience in practical applications of the present total DR rate coefficients, we fit them with the formula

$$\alpha^{\rm DR}(T) = \frac{1}{T^{3/2}} \sum_{i=1}^{k} C_i \exp(-E_i/T), \qquad (4)$$

with $k \le 5$. In this equation T and E_i are in Kelvin and the rate coefficients α have units cm^3/s. Table 3 presents the list of coefficients C_i and E_i for all ions of the He-like sequence considered here. The fits are accurate to better than 1% up to $z^2 10^7$ K and down to the temperature at which the peak rate coefficient has fallen-off by at least five orders of magnitude.

3.3. Level-specific DR recombination coefficients

In Fig. 6 we present final n-resolved rate coefficients for a sample of ions. Of course, there exists hundreds of final levels for each ion; though here we only plot sums of LSJ levels onto total n-resolved states. Here we can see that DR is dominated in all cases by recombination onto $n = 2$ and 3 states, while recombination onto higher orbitals decreases monotonically.

All partial (final-state level-resolved) and total rate coefficients are tabulated over $z^2(10–10^7)$ K in the *adf09* format (Summers 2003) and made available online at the Oak Ridge Controlled Fusion Atomic Data Center at `http://www-cfadc.phy.ornl.gov/`. Also, the data will be included in the XSTAR database (Bautista & Kallman 2001).

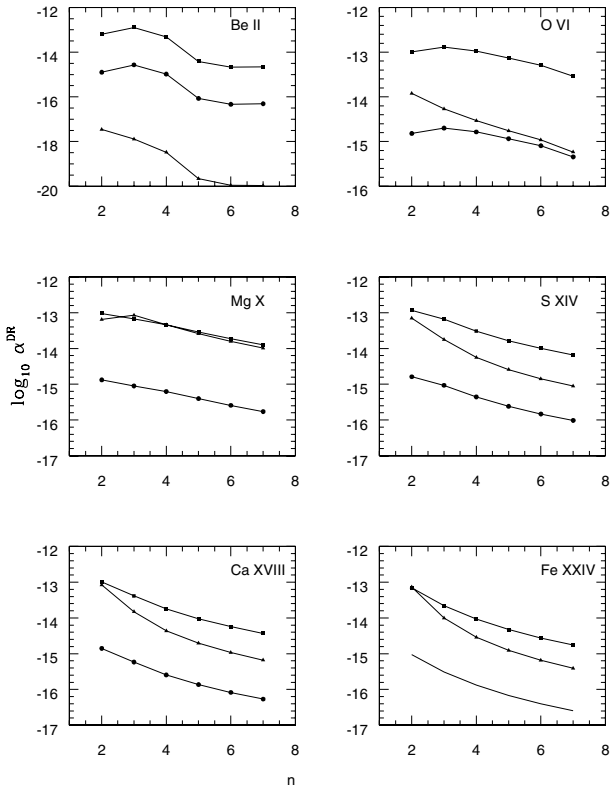

Fig. 6. Recombination rate coefficients vs. orbital quantum number n. The temperatures considered are 2×10^4 z^2 (triangular dots), 5×10^5 z^2 (square dots), and 10^7 z^2 (circular dots) K.

4. Spectral modelling of Li-like species

As an illustration for the use of the atomic data, we model the spectra of Li-like ions under low density conditions, including the effects of collisional excitation, radiative decay, photoionization, radiative and dielectronic recombination, and collisional ionization. Thus, the population of any level n_i is given by

$$n_i \sum_{i\neq i} \left(A_{ij} + N_{\rm e}C^{\rm e}_{ij} + +N_{\rm e}Q_{i\infty} + \Gamma_i\right) = \sum_{k<i} n_k A_{ki}$$
$$+ \sum_{l<i} n_l N_{\rm e} C^{\rm e}_{li} N^+ N_{\rm e}\alpha_i + N^+ N^2_{\rm e} C_{\infty i}$$

where A_{ij} is the radiative transition rate from level i to level j; $N_{\rm e}$ and $C^{\rm e}_{ij}$ are the density per unit volume of electrons and the transition rates by collisions with electrons respectively; Γ_i is the photoionization rate out of level i; N^+ is the density of the next ionization stage of the element, i.e. the He-like ionic state in this case. α_i is the rate coefficient for recombination (radiative plus dielectronic) to level i. $C_{i\infty}$ and $C_{\infty i}$ are the collisional ionization and 3-body recombination rate coefficients respectively. In principle, the sums in this equation includes energy levels 1 through infinity. For the present models we explicitly include all levels up to $n = 5$ followed by unphysical "superlevels" built to account for the contributions of higher energy levels. For radiative recombination in these models we employ the partial rate coefficients of Badnell (2006a).

Recombination contributions to emission spectra of Li-like ions are expected to be greater under conditions found in photoionized plasmas because their equilibrium temperatures for a given ionization structure are lower than in the case of coronal plasmas. The lower temperatures favour recombination rates relative to collisional excitation.

Figure 7 compares the resulting spectra from Fe XXIV with and without contributions from recombination. The ionization structure and equilibrium temperature were computed with the photoionization modelling code XSTAR v.2 (Kallman & Bautista 2001) for a typical, solar composition, astrophysical plasma. In all cases the recombination contributions to the dominant 2p−2s and 3p−2s lines are small, only a few percent. Yet, recombination can lead to a number of weak lines that often appear as unresolved pseudo-continuum in observed spectra. Such recombination lines become dominant towards the low and high ionization parameters/temperature where the ionization fractions of Li- and He-like species are small, while recombination contributions seem negligible under conditions of where the Li-like/He-like stages peak.

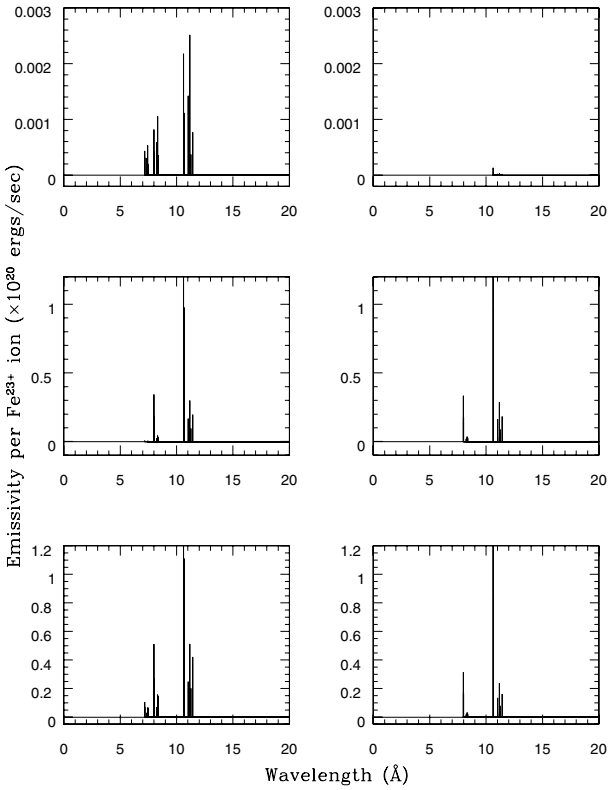

Fig. 7. Emission spectra from Li-like iron in a photoionized plasma with solar composition. *Panel on the right hand side* depict the spectra from pure collisional excitation while spectra in the left include the contributions from recombination. The various spectra correspond to photoionization equilibrium conditions (log χ, $T_{\rm e}$, $\chi(Fe^{23+})$, $\chi(Fe^{24+})$ = (2.5, 7.58×10^5 K, 2.7×10^{-3}, 6.6×10^{-5}) for the *upper panels*, (3.5, 2.37×10^7 K, 9.6×10^{-2}, 0.41) for the *middle panels*, and (5, 8.23×10^7 K, 2.3×10^{-5}, 9.3×10^{-3}) for the *lower panels*.

5. Summary

We have computed total and final-state level-resolved DR rate coefficients for a large number of He-like ions of practical interest in astrophysical and laboratory fusion plasmas. The calculation were performed in the isolated resonance approximation using the Thomas-Fermi-Dirac model potential. The calculations were done both in *LS* and relativistic intermediate coupling schemes.

We find that while IC effects are insignificant for total DR rates these effects do become very large for level specific rates. Thus, IC DR rate coefficients should always be used in spectral modelling of finite density plasmas.

The present DR rate coefficients agree well with experimental determinations and with the data compiled by M98, with the exception of the rates for Li^+. In this latter case the differences are approximately one order of magnitude.

We have modelled the emission spectra of Li-like ions including the contribution of recombination from the He-like stages for low-density photoionized plasmas. Under these conditions the contributions from recombination to the spectrum are small. Nonetheless, recombination plays a fundamental role for high-density plasmas, beyond the critical density for collisional excitation of the dominant resonant transitions in the spectrum. Modelling of such situations requires detail treatment of effects like thermalization of excited levels and lowering of the continuum on a case-by-case basis (see Bautista & Kallman 2000).

The archived database is suitable for the modelling of dynamic and/or finite density plasmas over a wide range of plasma timescales and electron densities. A start has now been made on M-shell sequences, e.g. Na- and Mg-like Altun et al. (2006, 2007), and specific ions, e.g. Fe $3p^q$ Badnell (2006b).

References

Abdallah, J., & Clark, R. E. H. 1994, J. Phys. B, 27, 3589
Altun, Z., Yumak, A., Badnell, N. R., et al. 2006, A&A, 447, 1165
Altun, Z., Yumak, A., Badnell, N. R., et al. 2007, A&A, to be submitted
Ali, R., Bhalla, C. P., Cocke, et al. 1990, Phys. Rev. Lett., 64, 633
Ali, R., Bhalla, C. P., Cocke, C. L., et al. 1991, Phys. Rev. A, 44, 223
Andersen, L. H., Hvelplund, P., Knudsen, H., & Kvistgaard, P. 1989, Phys. Rev. Lett., 62, 2656
Andersen, L. H., Bolko, J., & Kvistgaard, P. 1990, Phys. Rev. A, 41, 1293
Andersen, L. H., Pan, G. Y., Schmidt, H. T., et al. 1992, Phys. Rev. A, 45, 7868
Badnell, N. R. 1986, J. Phys. B, 19, 3827
Badnell, N. R. 1988, J. Phys. B, 21, 749
Badnell, N. R. 1997, J. Phys. B, 30, 1

Badnell, N. R. 2006a, ApJS, 167, 334
Badnell, N. R. 2006b, AJ, 651, L73
Badnell, N. R., & Pindzola, M. S. 1989, Phys. Rev. A, 39, 1685
Badnell, N. R., Pindzola, M. S., & Griffin, D. C. 1990, Phys. Rev. A, 41, 2422
Badnell, N. R., Gorczyca, T. W., & Price, A. D. 1998, J. Phys. B, 31, L239
Badnell, N. R., O'Mullane, M. G., Summers, H. P., et al. 2003, A&A, 406, 1151
Bartsch, T., Müller, A., Spies, W., et al. 1997, Phys. Rev. Lett., 79, 2233
Bautista, M. A., & Kallman, T. R. 2000, ApJ, 544, 581
Bautista, M. A., & Kallman, T. R. 2001, ApJS, 134, 139
Bautista, M. A., Kallman, T. R., Angelini, L., et al. 1998, ApJ, 509, 848
Beiersdorfer, P., Phillips, T. W., Wong, K. L., et al. 1992, Phys. Rev. A, 46, 3812
Bely-Dubau, F., Gabriel, A. H., & Volonté, S. 1979, MNRAS, 186, 405
Burgess, A. 1964, ApJ, 139, L776
Burgess, A. 1965, ApJ, 141, 1588
Chen, M. H. 1986, Phys. Rev. A, 33, 1986
Chen, M. H. 1988, Phys. Rev. A, 38, 6430
Dewitt, D. R., Scheider, D., Clark, M. W., et al. 1991, Phys. Rev. A, 44, 7185
Eissner, W., & Nussbaumer, H. 1969, J. Phys. B, 2, 1028
Eissner, W., Jones, M., & Nussbaumer, H. 1974, Comput. Phys. Commun., 8, 270
Gorczyca, T. W., & Badnell, N. R. 1996, Phys. Rev. A, 54, 4113
Gorczyca, T. W., & Badnell, N. R. 1997, Phys. Rev. Lett., 79, 2783
Gorczyca, T. W., Badnell, N. R., & Savin, D. W. 2002, Phys. Rev. A, 65, 062707
Gu, M. F. 2003, ApJ, 590, 1131
Heeter, R. F., Emig, J. A., Foord, M. E., et al. 2000, in Atomic Data Needs for X-ray Astronomy, ed. M. A. Bautista, T. R. Kallman, & A. K. Pradhan, NASA/CP-2000-209968, 135
Kallman, T. R., & Bautista, M. A. 2001, ApJS, 133, 221
Kenntner, J., Broude, C., Habs, D., et al. 1995, Nucl. Instrum. Methods Phys. Res., B98, 142
Kilgus, G., Berger, J. M., Blatt, P., et al. 1990, Phys. Rev. Lett., 64, 737
Kilgus, G., Habs, D., & Wolf, A. 1993, Phys. Rev. A, 47, 4859
Knapp, D. A., Marrs, R. E., Schneider, M. B., et al. 1993, Phys. Rev. A., 47, 2039
Mannervik, S., DeWitt, D., Engström, L., et al. 1998, Phys. Rev. Lett., 81, 313
Marchuk, O., Bertschinger, G., Kunze, H.-J., et al. 2004, J. Phys. B, 37, 1951
Mazzotta, P., Mazzitelli, G., Colafrancesco, S., & Vittorio, N. 1998, A&AS, 133, 403
Nahar, S. N. 1999, ApJS, 120, 131
Nahar, S. N., & Pradhan, A. K. 1997, ApJS, 111, 339
Nahar, S. N., Pradhan, A. K., & Zhang, H. L. 2000, ApJS, 131, 375
Nahar, S. N., Pradhan, A. K., & Zhang, H. L. 2001, ApJS, 133, 255
NIST 2002, http://www.nist.gov/PhysRefData/ASD/levels_form.html
Nussbaumer, H., & Storey, P. J. 1983, A&A, 126, 75
O'Rourke, B. E., Kuramoto, H., Li, Y. M., et al. 2004, J. Phys. B, 37, 2343
Pindzola, M. S., & Badnell, N. R. 1992, Nucl. Fusion and Plasma Material Interaction data for fusion, 3, 101
Pindzola, M. S., Badnell, N. R., & Griffin, D. C. 1992, Phys. Rev. A, 46, 5725
Price, A. D. 1997, Ph.D. Dissertation, University of Strathclyde
Saghiri, A. A., Linkemann, J., Schmitt, M., et al. 1999, Phys. Rev. A, 60, 3350
Savin, D. W. 1999, ApJ, 523, 855
Savin, D. W., & Laming, J. M. 2002, ApJ, 566, 1166
Summers, H. P. 2003, ADAS User manual (Version 2.6) http://adas.phys.strath.ac.uk
Summers, H. P., Badnell, N. R., O'Mullane, M. G., et al. 2002, Plasma. Phys. Control. Fusion, 44, B323
Verner, D. A., & Ferland, G. A. 1996, ApJS, 103, 467
Závodszky, P. A., Houck, J. H., Tanis, J. A., et al. 1998, Phys. Rev. A, 58, 2001
Zhang, H. L., Nahar, S. N., & Pradhan, A. K. 1999, J. Phys. B, 32, 1459
Zong, W., Schuch, R., Gao, H., et al. 1998, J. Phys. B, 31, 3729